Presynaptic calcium currents and their relation to synaptic transmission: Voltage clamp study in squid giant synapse and theoretical model for the calcium gate

(mathematical model/3-aminopyridine)

RODOLFO LLINÁS, IZCHAK Z. STEINBERG*, AND KERRY WALTON

Division of Neurobiology, University of Iowa, Oakdale Iowa 52319, and Neurosciences Research Program, Massachusetts Institute of Technology, Boston, Mass. 02130

ABSTRACT A voltage clamp study of the presynaptic terminal in squid stellate ganglion has given quantitative results relating inward Ca^{2+} current to presynaptic membrane potential and postsynaptic response to inward Ca^{2+} current. The results indicate an S-shaped curve for the relationship between presynaptic potential and Ca^{2+} current and a linear relationship between Ca^{2+} current and postsynaptic potential. A similar S-shaped curve was found for the time-dependent properties of the Ca^{2+} conductance. Based on these results a mathematical model was developed which accounts for the experimental results in this and previously published papers by other authors. The model suggests that five subunits are involved in the Ca^{2+} gate and that the subunits change noncooperatively from an inactive to an active form upon membrane depolarization.

Recent studies have indicated that Ca^{2+} is the essential ion in the mediation of potential-dependent release of transmitter from the presynaptic terminal in squid stellate ganglion (1–4). These qualitative studies have shown that depolarization of the presynaptic terminal releases transmitter by the activation of a Ca^{2+} conductance change resulting in a flow of Ca^{2+} into the pre-synapse. Little is known, however, about quantitative parameters relating presynaptic depolarization to inward Ca^{2+} current. While Ca^{2+} current (I_{Ca}) has been measured by a diversity of techniques in the squid postsynaptic fiber, the giant axon (5–8), to our knowledge the only measurement relating activation of the "late Ca^{2+} channel" to potential is that of Baker et al. (6) using aequorin light emission as a probe. Voltage clamp experiments in the postsynaptic axon have determined, on the other hand, that in this structure the late I_{Ca} is probably too small to be measured electrophysiologically, its amplitude being apparently beyond the resolution of the measuring systems (7).

In the presynaptic terminal, however, it has been found that I_{Ca} is larger than that in the postsynaptic fiber. Thus, Ca^{2+} spikes may be produced following Na^+ and K^+ blockage only in the presynaptic fiber (9, 10). Furthermore, measurements with intracellular aequorin show light emission from this terminal (2–4) at extracellular Ca^{2+} concentration levels too low to generate a detectable light level under similar conditions at the postsynaptic fiber (6).

This paper presents experimental data concerning the amplitude, time course, and kinetics of I_{Ca} and their relation to synaptic transmission. A model for the potential-dependent Ca^{2+} conductance change is developed on the basis of thermodynamic considerations and of kinetic properties extracted from experimental results. The model suggests that the Ca^{2+} channel is formed by five monomers, each having one gating

Abbreviation: I_{Ca}, calcium current.
* Permanent address: Dept. of Chemical Physics, Weizmann Institute of Science, Rehovot, Israel.

charge and capable of assuming in a noncooperative manner a molecular structure which permits Ca^{2+} flow through the channel.

MATERIALS AND METHODS

Experiments were conducted at the Marine Biological Laboratory at Woods Hole, Mass. Stellate ganglia from *Loligo pealii* were dissected and isolated from the mantle and placed in oxygenated artificial sea water containing 450 mM Na^+, 20 mM Mg^{2+}, *40* mM Ca^{2+}, 10 mM K^+, with Cl^- as the anion. The artificial sea water was buffered at pH 7.2 with sodium bicarbonate.

The presynaptic terminal was penetrated with two micropipettes with a resistance of 5–10 MΩ which were checked for linearity during current injection. The postsynaptic potential was measured with a third micropipette inserted at the site of synaptic junction. Voltage clamp was attained with the circuits shown in Fig. 1A. The voltage obtained by the recording electrode (Em) was inverted and fed back through a 100-gain amplifier with a maximum voltage output of 100 V. Voltage clamp was attained after blocking Na^+ current with 10 μg/ml of tetrodotoxin (11) and reducing K^+ conductance with 5 mM 3-aminopyridine (10, 12, 13). Following administration of these drugs, the voltage clamp state could be attained in approximately 250 μsec. Presynaptic polarization levels remained fairly linear up to approximately +10 mV absolute membrane potential level. Beyond this point, a sizeable outward K^+ current was detected (13).

Although this type of point voltage clamp cannot provide a condition of isopotentiality along the presynaptic terminal, a preliminary set of measurements indicates that, at the levels utilized, the degree of isopotentiality between the site of injection and the recording site was no more than 10% in error. The current was measured through the bath electrode by means of a 5-gain operational amplifier.

A mathematical model developed from the experimental results was implemented in a PDP-15 (Digital Equipment Corp.) computer and the simulated results were displayed through a PDP-15 graphics system.

RESULTS

Voltage clamp experiments yielded the type of records shown in Fig. 1B. Presynaptic voltages are indicated in the upper trace, inward presynaptic currents generated by the voltage steps are shown in the middle trace, and postsynaptic responses are illustrated in the lower trace. A sample of typical voltage–peak current relationships encountered in the presynaptic terminal is shown in Fig. 1C. Presynaptic current is related in an S-shaped manner to presynaptic potential at levels tested in the

Physiology: Llinás *et al.*
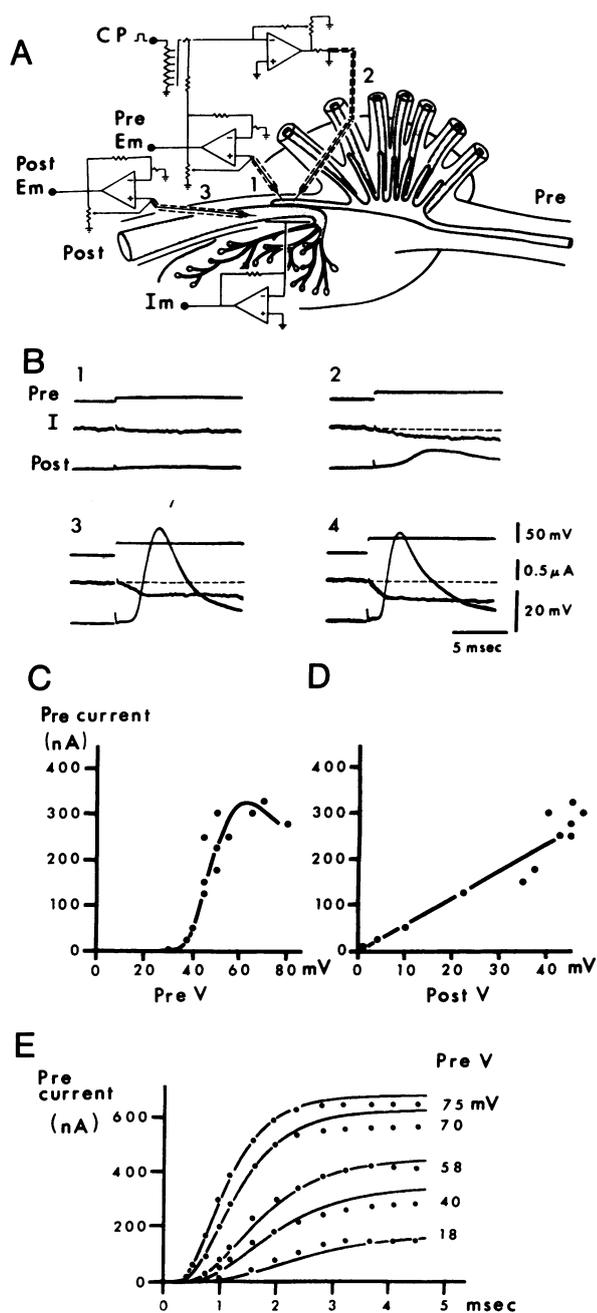
Proc. Natl. Acad. Sci. USA 73 (1976) 2919

FIG. 1. Relationships between presynaptic depolarization, inward I_{Ca} current in the pre-terminal, and postsynaptic response. (A) Diagram of experimental setup. The pre-terminal is impaled with two electrodes; one, 1, records potential, the second, 2, injects current through a feedback amplifier. Command pulses (CP) are introduced through the same amplifier. Postsynaptic potential is measured (Post Em) through a third electrode, 3. Transmembrane current (Im) is measured across an external bath electrode as shown in the illustration. (B) Results obtained after pharmacological blocking of Na^+ and K^+ conductances. Records 1–4 show different levels of presynaptic voltage clamping. The upper traces show presynaptic potentials; the middle, presynaptic currents; and the lower, postsynaptic potentials. As the presynaptic potential is increased from 1–4, a sustained inward current is observed (middle trace), accompanied by a postsynaptic response. (C) Plot of peak inward current (ordinate in nA) against presynaptic depolarization. (D) Plot of presynaptic inward current (ordinate) against amplitude of the postsynaptic potential. (E) The kinetics of inward I_{Ca} experimentally determined at different membrane potentials in a second preparation (dots). The continuous lines represent the computer printouts of the kinetics obtained from the proposed model.

present experiments. Membrane depolarizations beyond the values indicated could not be obtained with 3-aminopyridine because the K^+ conductance blockage is voltage-dependent (10, 12, 13).

The relationship between presynaptic current and postsynaptic response was found to be close to linear (Fig. 1D) up to the level where nonlinearities due to the size of the postsynaptic response became prevalent (14). That these currents are calcium dependent was demonstrated by removal of Ca^{2+} from the bathing solution. Under these conditions, synaptic transmission was blocked (15) and no inward current was observed.

The time-dependent inward Ca^{2+} flow during a constant postsynaptic voltage step is presented in Fig. 1E. This inward flow is illustrated for various degrees of membrane polarization. One of the striking features of the curves is the lag period that precedes the rapid rise in I_{Ca}. This current eventually reaches a stationary value that depends on the membrane potential.

The actual mechanism responsible for the potential-dependent Ca^{2+} influx—whether it involves a transport protein, a channel, or something else—is as yet unclear. In the following we shall refer to it as the "Ca^{2+} gate". Whatever the nature of the gate, it must fulfill the special set of kinetic requirements indicated by the experimental data in Fig. 1. These requirements were successfully met by assuming that a set of intermediary steps precedes the opening of the Ca^{2+} gates upon changing the membrane potential. A model was thus developed which accounts for our empirical data and resembles, in general lines, that of Hodgkin and Huxley (16) for the K^+ currents.[†]

It is assumed that each Ca^{2+} gate is made up of n subunits, which may be in one of two forms, S and S', the gate being open if all n subunits are in the S' form. No mutual influence on the S or S' forms of a subunit by its neighbors is assumed. The system may thus be described by the following scheme:

$$S \underset{k_2}{\overset{k_1}{\rightleftharpoons}} S'; \quad nS \longleftrightarrow G$$
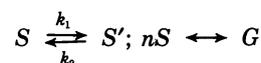
where k_1 and k_2 are the forward and backward rate constants for the conversion of S into S', and G designates an open gate. If we start at zero time with a system in which no gates are open, i.e., $[G] = 0$, and therefore $[S'] = 0$, the increment of S' with time will be given by

$$[S'] = [S]_0 \frac{k_1}{k_1 + k_2} [1 - \exp \{-(k_1 + k_2)t\}] \quad [1]$$

where S_0 is the total number of subunits, whether in form S or S'. The probability that a subunit is in form S' is obviously $[S']/[S]_0$; the probability $[G]/[G]_0$ that a given gate is open, i.e., has all its n subunits in the S' form, is $([S']/[S]_0)^n$. (G_0 is the total number of gates, whether open or closed.) Thus:

$$\frac{[G]}{[G]_0} = \left[\frac{k_1}{k_1 + k_2} [1 - \exp \{-(k_1 + k_2)t\}] \right]^n \quad [2]$$

Since I_{Ca} is potential-dependent (Fig. 1E), it follows that k_1 and k_2 must also be so. Such a dependence may occur if the charge distribution in S or S' is different from that of the activated transition state for the $S \rightleftharpoons S'$ transformation. The contribution of the membrane potential, V, to the energies of activation of the reactions corresponding to k_1 and k_2 will be $z_1 \epsilon V = (p - p_1)V/l$ and $z_2 \epsilon V = (p - p_2)V/l$, respectively, where ϵ is the (positive) elementary electric charge, l is the thickness of the membrane, and p, p_1, and p_2 are the dipole moments in the membrane of the activated transition state and of S and of S',

[†] For a review of related models for Na^+ and K^+ currents, see the recent volume by Jack *et al.* (17).

respectively, perpendicular to the membrane plane. The symbols z_1 and z_2 designate the number of charges that will have to move across the width of the membrane on transforming S and S', respectively, into the activated state to produce an equivalent dependence on V. The dependence of k_1 and k_2 on V will thus be:

$$k_1 = k_1{}^0 \exp (\epsilon z k_1 V/kT); \quad k_2 = k_2{}^0(\epsilon z_2 V/kT) \qquad [3]$$

where $k_1{}^0$ and $k_2{}^0$ do not depend on the membrane potential, k is Boltzmann's constant, and T is the absolute temperature.

The I_{Ca} is equal to the number of open gates, $[G]$, at the moment of interest, t, multiplied by the flow, j, of Ca^{2+} ions per unit time through a single open gate. The flow, j, can be obtained from the relation $j = -D(dc/dx) + (2\epsilon/f)cE$ by solving the differential equation which governs the distribution of Ca^{2+} concentration, c, in the membrane:

$$\frac{\partial c}{\partial t} = D\frac{\partial^2 c}{\partial x^2} - \frac{2\epsilon}{f}\frac{\partial (cE)}{\partial x} \qquad [4]$$

where D and f are the Ca^{2+} diffusion and frictional coefficients respectively ($f = RT/D$, R being the gas constant), x is the coordinate perpendicular to the membrane, and E is the electric field at point x in the membrane. The concentration c in the membrane can be assumed to be at steady state, i.e., $\partial c/\partial t = 0$. Solving Eq. 4 subject to the boundary conditions, $c = c_i$ inside the presynaptic terminal and $c = c_o$ outside the fiber, gives an expression for j:

$$j = \frac{c_i - c_o \exp (-2\epsilon V/kT)}{1 - \exp (-2\epsilon V/kT)} \cdot \frac{2D\epsilon}{kT} \cdot \frac{A}{l} V \qquad [5]$$

A is the cross-sectional area of the gate. In the derivation of Eq. 5, D and E are considered to be constant along x. The flow j decreases continuously with membrane depolarization and reverses sign at equilibrium potential (Fig. 2A, dotted curve). The I_{Ca} is thus

$$I_{Ca} = [G] \cdot j = [G]_0 \left[\frac{k_1}{k_1 + k_2}\{1 - \exp (-(k_1 + k_2)t)\}\right]^n$$
$$\times \frac{c_i - c_o \exp (-2\epsilon V/kT)}{1 - \exp (-2\epsilon V/kT)} \cdot \frac{2D\epsilon}{kT} \cdot \frac{A}{l} V \qquad [6]$$

with the rate constants k_1 and k_2 obeying Eq. 3. In Eq. 6 the values for $[G]_0$, D, and A are not known; however, these quantities only determine the height of the curves of I_{Ca} versus t and not their shape. The parameters determining the shape of these plots are k_1 (i.e., $k_1{}^0$ and z_1), k_2 (i.e., $k_2{}^0$ and z_2), and n. Families of curves with different values of these parameters were computer plotted and compared directly with the experimental data. The following values were found to fit best[‡]: $n = 5$, $z_1 = 1$, $z_2 = 0$, $k_1{}^0 = 2$ msec^{-1}, $k_2{}^0 = 1$ msec^{-1}. The smooth curves in Fig. 1E were calculated using these values for the parameters in Eq. 6. The fit to experimental results (Fig. 1E) is seen to be good and suggests that the gate has five subunits. While k_2 is independent of V, k_1 rises exponentially with membrane depolarization. In addition, since the equilibrium constant $[S']/[S]$ is equal to k_1/k_2, and $z_1 = 1$ and $z_2 = 0$, both S' and the activated intermediate state must have a dipole moment component along the field that is different from that of S by one positive charge equivalent moving outward across the membrane. This means that opening of a single gate must be associated with a gating current (18) equivalent to an outward displacement of five positive charges.

The constant values $I_{Ca}{}^\infty$ reached for I_{Ca} after applying a defined membrane potential for sufficient time (see Fig. 1E) are associated with reaching the equilibrium concentration of open gates at the specified membrane potential. $I_{Ca}{}^\infty$ is readily obtained from Eq. 6 by substituting in it $t = \infty$. Thus

$$I_{Ca}{}^\infty = [G]_0\left(\frac{k_1}{k_1 + k_2}\right)^n \frac{c_i - c_o \exp (-2\epsilon V/kT)}{1 - \exp (-2\epsilon V/kT)} \cdot \frac{2D\epsilon}{kT} \cdot \frac{A}{l} \cdot V$$

$$= [G]_0\left(\frac{(k_1{}^0/k_2{}^0) \exp [(z_1 - z_2)\epsilon V/kT]}{(k_1{}^0/k_2{}^0) \exp [(z_1 - z_2)\epsilon V/kT + 1]}\right)^n$$

$$\cdot \frac{c_i - c_o \exp (-2\epsilon V/kT)}{1 - \exp (-2\epsilon V/kT)} \cdot \frac{2D\epsilon}{kT} \cdot \frac{A}{l} \cdot V \qquad [7]$$

Eq. 7 was plotted for various values of the parameters n, $z_1 - z_2$, and $k_1{}^0/k_2{}^0$. The effect of varying n is illustrated in Fig. 2A. The results were compared with the equilibrium values of $I_{Ca}{}^\infty$ for various membrane potentials. The best fit was obtained for $n = 5$, $z_1 - z_2 = 1$, and $k_1{}^0/k_2{}^0 = 2$. The result is shown in Fig. 2B, in which the smooth line describes Eq. 7 with the above parameters. The agreement with our experimental data (Fig. 2B, filled circles) is seen to be excellent.[§] Good agreement is also obtained with the data of Baker *et al.* (6) (Fig. 2B, open circles). The fall-off of I_{Ca} at higher values of V is due to the decrease in the Ca^{2+} electromotive force, as expressed by j.

Eq. 2 cannot be utilized directly to evaluate the time course of I_{Ca} when the membrane potential is not constant, since it supposes that k_1 and k_2 are constant with time. As found above, however, k_1 will vary with time if the membrane potential changes. Under such circumstances the following procedure may be utilized:

The scheme $S \underset{k_2}{\overset{k_1}{\rightleftarrows}} S'$ implies that

$$\frac{d[\bar{S}]}{dt} = -(k_1 + k_2)[\bar{S}] + k_1$$

where $[\bar{S}] = [S']/[S]_0$. Multiplying by $5[\bar{S}]^4$ and following standard substitutions, one obtains:

$$\frac{d[\bar{G}]}{dt} = -5(k_1 + k_2)[\bar{G}] + 5k_1[\bar{G}]^{4/5} \qquad [8]$$

Eq. 8 can be integrated numerically in a stepwise way with k_1 (or k_2) varying with time. The flow I_{Ca} is then obtained from the relation $I_{Ca} = [G] \cdot j$ by combining the solution of Eq. 8 with Eq. 5.

The numerical solution for I_{Ca} when the membrane potential was varied so as to reproduce a presynaptic action potential is illustrated in Fig. 2C. Solving Eq. 8 gives the gate formation (a), and multiplying this by Eq. 5 gives the Ca^{2+} current (b) produced by the action potential. Since it was experimentally determined that the postsynaptic response is related linearly to the presynaptic current and begins approximately 200 μsec after the onset of I_{Ca} (19), curve (b) was appropriately delayed and amplified to give the synaptic current (c). The synaptic potential (d) was obtained as the product of (c) across a distributed resistive and capacitative network with parameters similar to those found in the postsynaptic axon (16).

The results in Fig. 2C indicate that the time course and delay of the postsynaptic potential seen under these circumstances are similar to those observed experimentally. Furthermore,

---

[‡] Values of 4 and 6 for n did not fit as well but cannot be ruled out.

[§] The shape of $I_{Ca}{}^\infty$ is dictated by only three parameters [n, $k_1{}^0/k_2{}^0$, and ($z_1 - z_2$)] compared to five for I_{Ca}, Eq. 6. To facilitate the evaluation of the parameters we have in practice fitted first Eq. 7 to the measured $I_{Ca}{}^\infty$ data, thus obtaining n, $k_1{}^0/k_2{}^0$, and ($z_1 - z_2$). By use of this information, the analysis of the kinetic data (Fig. 1E) in terms of Eq. 6 was much simplified.
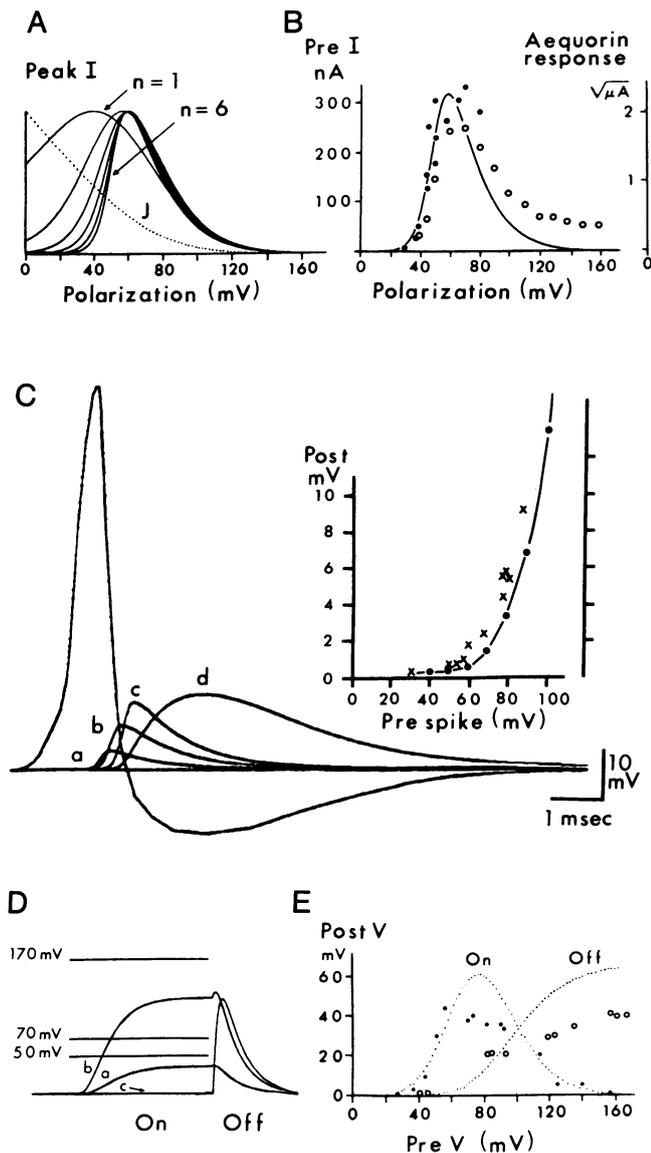
Physiology: Llinás *et al.*

Proc. Natl. Acad. Sci. USA 73 (1976) 2921

FIG. 3. Schematic representation of hypothetical Ca²⁺ channel. (A) Side-view showing longitudinal section of channel, which consists of five monomers extending the thickness of the membrane. On the left is a channel at rest with a charge distribution such that each monomer is positive at the inner, and negative at the outer, membrane surface (shown in left monomer). The middle section shows an intermediate state following a change in the electric field across the membrane (membrane polarization). The charge redistribution in each monomer is assumed to produce a conformational change (S to S') such that a "trap", indicated by a deformity of the molecule that obstructs the channel, is removed. Extreme right portion of diagram shows an open channel (G form) when the conformational change of all five monomers is accomplished, allowing Ca²⁺ to flow across the membrane. (B) Front view of channel from inward membrane surface.

FIG. 2. Graphic solutions to Eqs. 5, 6, 7, and 8, demonstrating the properties of the model and comparing them to experimental data. (A) Solid lines: $I_{Ca}°$ determined from Eq. 6 for $n = 1$ to $n = 6$ for different levels of depolarization, an n of 5 being the best fit for the data; dotted line: solution to Eq. 5. (B) Experimental results obtained from the present voltage clamp study (●) and the data of Baker *et al.* (6) (○) are superimposed on printout for $n = 5$. The ordinates are current in nA and the square root of light emission. (C) Reconstruction of events during synaptic transmission by means of Eqs. 5 and 8. The presynaptic action potential used in the calculation was experimentally obtained. The four curves that follow represent (a) time course of Ca²⁺ gate formation, (b) time course of Ca²⁺ current, (c) time course of postsynaptic current, and (d) postsynaptic potential (arbitrary scale). In the plot to the right the amplitude of presynaptic action potential is varied. Computer results (●) are compared with those obtained experimentally (✕) (20) under these conditions. Right ordinate: amplitude of computed synaptic potential on an arbitrary scale; left ordinate: amplitude of experimental results in mV (20). For further explanation, see *text*. (D) Solution for I_{Ca} using Eqs. 5 and 8, showing properties of the on–off response and the so-called synaptic suppression phenomenon. Three square voltage pulses of increasing amplitude generate results (a), (b), and (c), respectively (amplitude in arbitrary units). In (c) only the off response is present. (E) Plot comparing numerical results for on–off curves (dots) on an arbitrary scale with experimental data in mV (on: ●; off: ○). The divergence of the experimental and computer results is due to the nonlinear properties of the postsynaptic response above 40 mV.
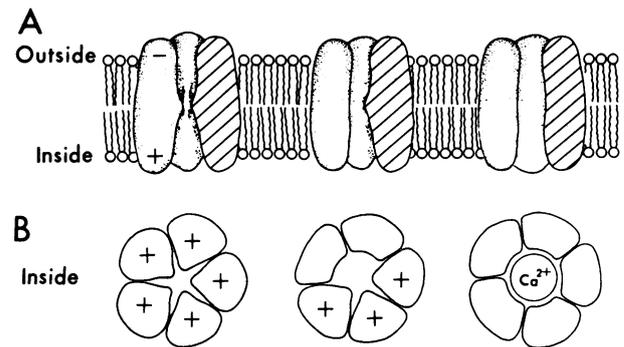
when the amplitude of the presynaptic action potential is modified, the postsynaptic responses obtained are exactly those encountered experimentally by Takeuchi and Takeuchi (20) (inset of Fig. 2C). If, instead of an action potential, a square wave of depolarization is introduced, the well-known phenomenon of synaptic suppression (1, 21, 4) is observed (Fig. 2D). The on–off properties of the postsynaptic response under these conditions are quite similar to those encountered experimentally (Fig. 2E). The latency differences for the on and off release (19) were also reproduced (Fig. 2D).

DISCUSSION

The results presented in this communication quantitatively relate inward I_{Ca} and transmitter release to presynaptic depolarization. Among the more striking findings is the S-shaped relation between presynaptic voltage and I_{Ca}. This nonlinearity is similar to that reported by Baker *et al.* (6), who used aequorin to detect I_{Ca} in the postsynaptic axon. In addition, for given membrane polarizations our data indicate an S-shaped curve for the kinetics of Ca²⁺ inflow. These data can be quantitatively accounted for in a self-consistent way by the present model (Fig. 3), which we feel may represent a general solution to the potential-dependent Ca²⁺ conductance changes in different cell membranes.

The postsynaptic response was found to be linearly related to the Ca²⁺ current, suggesting that the transmitter release is proportional to the inward I_{Ca}. If this release brought about by discharge from vesicles according to the quantal hypothesis (22) is triggered by binding of Ca²⁺ to a specific site (presumably on a protein molecule), our results imply that the binding of a single Ca²⁺ ion suffices for a discharge of one quantum of transmitter. This is at variance with the conclusions of Dodge and Rahamimoff (23) that the binding of four Ca²⁺ ions is required for this purpose.

Since the latency of the onset of transmitter release following the "off" inflow of Ca²⁺ is as short as 200 μsec (19), the events following Ca²⁺ entry that culminate in postsynaptic response must all occur within this short lapse of time. Even if the only

variable of significance were to be the radius of action of Ca^{2+} ions intracellularly, the small diffusion coefficient of this ion (10^{-7} cm^2/sec) (5) suggests that Ca^{2+} must cross the membrane very close to, or at the very site of, transmitter release. Thus, only those vesicles immediately adjacent to the membrane, or in actual contact with it, are probably affected by this Ca^{2+} inflow. The short latency for the off-release also suggests that synaptic delay is mainly related to the time dependence of I_{Ca}.

The present experimental results indicate no inactivation of the Ca^{2+} conductance for the time range investigated. This lack of inactivation may, however, be related to the action of 3-aminopyridine which, as in the case of tetraethylammonium, may enhance the Ca^{2+} conductance and prevent its inactivation (24). It is questionable whether this form of inactivation plays a role in normal synaptic transmission. In fact, although our model is derived from data obtained in the presence of 3-aminopyridine, it is also consistent with results obtained in the absence of such pharmacological agents (see Fig. 2C). That the inactivation of Ca^{2+} conductance may in fact be present is, however, important when considering longer-lasting modulation of transmitter release.

1. Katz, B. & Miledi, R. (1967) *J. Physiol. (London)* **192**, 407–436.
2. Llinás, R., Blinks, J. R. & Nicholson, C. (1972) *Science* **176**, 1127–1129.
3. Miledi, R. (1973) *Proc. R. Soc. London Ser. B* **183**, 421–425.
4. Llinás, R. & Nicholson, C. (1975) *Proc. Natl. Acad. Sci. USA* **72**, 187–190.
5. Hodgkin, A. L. & Keynes, R. D. (1957) *J. Physiol. (London)* **138**, 253–281.
6. Baker, P. F., Hodgkin, A. L. & Ridgway, E. B. (1971) *J. Physiol. (London)* **218**, 709–755.
7. Meves, H. & Vogel, W. (1973) *J. Physiol. (London)* **235**, 225–265.
8. Rojas, E. & Taylor, R. E. (1975) *J. Physiol. (London)* **252**, 1–27.
9. Katz, B. & Miledi, R. (1969) *J. Physiol. (London)* **203**, 459–487.
10. Llinás, R., Walton, K. & Bohr, V. (1976) *Biophys. J.* **16**, 83–86.
11. Narahashi, T., Moore, J. W. & Scott, W. R. (1964) *J. Gen. Physiol.* **47**, 965–974.
12. Pelhate, M. & Pichon, Y. (1974) *J. Physiol. (London)* **242**, 90–91P.
13. Yeh, J. Z., Oxford, G. S., Wu, C. H. & Narahashi, T. (1976) *Biophys. J.* **16**, 77–81.
14. Boyd, I. A. & Martin, A. R. (1956) *J. Physiol. (London)* **132**, 74–91.
15. Miledi, R. & Slater, C. R. (1966) *J. Physiol. (London)* **184**, 473–498.
16. Hodgkin, A. L. & Huxley, A. F. (1952) *J. Physiol. (London)* **117**, 500–544.
17. Jack, J. J. B., Noble, D. & Tsien, R. W. (1975) *Electric Current Flow in Excitable Cells* (Clarendon Press, Oxford).
18. Armstrong, C. M. (1975) *Physiologist* **18**, 93–98.
19. Llinás, R., Walton, K. & Hess, R. (1976) *Fed. Proc.* **35**, 696.
20. Takeuchi, A. & Takeuchi, N. (1962). *J. Gen. Physiol.* **45**, 1181–1193.
21. Kusano, K., Livengood, D. R. & Werman, R. (1967) *J. Gen. Physiol.* **50**, 2579–2601.
22. Castillo, J. del & Katz, B. (1954) *J. Physiol. (London)* **124**, 560–573.
23. Dodge, F. A. & Rahamimoff, R. (1967) *J. Physiol. (London)* **193**, 419–432.
24. Kleinhaus, A. L. & Prichard, J. W. (1975) *J. Physiol. (London)* **246**, 351–361.